



Data fusion for air quality mapping using low-cost sensor observations: Feasibility and added-value



Alicia Gressent^{a,*}, Laure Malherbe^a, Augustin Colette^a, Hugo Rollin^a, Romain Scimia^b

^a Institut National de l'Environnement Industriel et des Risques (INERIS), France

^b AtmoTrack, France

ARTICLE INFO

Handling Editor: Xavier Querol

Keywords:

Air quality mapping
Low-cost sensors
Data fusion
 PM_{10}

ABSTRACT

In Nantes, low-cost sensors were installed in the city center and deployed on driving school cars, ambulances and service vehicles to measure PM_{10} concentrations. This work aims to use the large amount of observations provided by the sensors for air quality mapping at the urban scale in order to show the potential added-value with respect to the dispersion model (ADMS-Urban) calculations. A preprocessing is applied to the raw sensor dataset to remove the unreliable observations based on an outlier detection technique and to compensate for the measurement drift by adjusting the estimated daily variation of the underlying background PM_{10} concentrations with the reference stations. Then, data fusion is performed by combining the preprocessed fixed and mobile low-cost sensor observations and the 2016 annual average of the ADMS-Urban outputs. The measurement uncertainty related to the low-cost sensors and the dispersion of the data are considered in data fusion as the Variance of Measurement Error (VME). The spatial interpolation is achieved at hourly resolution and results are presented for November 29th, 2018 from 7 am to 7 pm. Hourly fused maps show disparate responses to data fusion mainly depending on the variability of the sensor data and the correlation between the sensor observations and the drift. The data fusion performance has been investigated by comparing the daily average of the estimated concentrations, the reference observations and the hourly model outputs at each station of the Air Pays de la Loire network. Results show that considering the model alone implies 8% bias whereas including the LCS observations reduces the bias to 2.5%. However, the concentration distributions related to the data fusion are characterized by a lower dispersion than the reference observations and the model estimation. Thus, the fusion smooths the PM_{10} peaks. In addition, the effect of the measurement uncertainty has been investigated by doubling it or reducing it to the reference station measurement uncertainty. The sensitivity study demonstrates that the performance is increasing by reducing the uncertainty. This highlights the importance to estimate accurately the measurement uncertainty of the devices to ensure relevant air quality mapping. The method efficiency is also quite limited by the low correlation between the sensor observations and the model used as external drift in the kriging that may be explained by the remaining bias on LCS data. Efforts on this issue might increase the performance of the spatial interpolation.

1. Introduction

The impact of outdoor air pollution on human health is overwhelming according to recent studies (Cohen et al., 2017; Burnett et al., 2018, 2014). The World Health Organization pointed out that 4.2 million deaths in the world are caused by the ambient air pollution (World Health Organization, 2014). For at-risk population, the particulate matter (PM), Ozone (O_3) and Nitrogen dioxide (NO_2) are known to exacerbate diseases (Sack and Goss, 2015; Landrigan et al., 2017). There is evidence that PM_{10} (particulate matter with a diameter of less than 10 μm) has a short-term exposure effect on respiratory health and it has been shown that $\text{PM}_{2.5}$ (particulate matter with a diameter of less

than 2.5 μm) is responsible for a high mortality rate in the 250 most populous cities worldwide (Anenberg et al., 2019). PM can be emitted directly or formed by chemical reactions in the atmosphere because of anthropogenic emissions (traffic, agriculture, or residential sources). To reduce its impact, it is necessary to mitigate its emissions and control its concentrations in the ambient air.

To meet this need, regulatory air quality monitoring has been established (see for instance the Air Quality in Europe report, European Environment Agency, 2019). Air quality monitoring is conventionally based on a network of stations allowing a continuous report of the pollutant concentrations at local and regional scales. Stations provide observations of the regulated pollutants (mainly NO_2 , SO_2 , O_3 , PM_{10} ,

* Corresponding author.

PM_{2.5}, benzene, PAHs and heavy metals). Their measurement uncertainty is constrained by the European legislation ([directive 2008/50/CE](#) and [2004/107/CE](#)) ensuring observation accuracy. They also must fulfill a criterion of time coverage depending on the pollutant and the type of measurement (fixed, indicative). Stations are classified depending on the nearby predominant emission sources (traffic, industrial and background stations). In addition to in situ observations, air quality modelling is used to estimate pollution especially at locations where there is no measurement station. Indeed, Chemistry Transport Models (CTM) and Gaussian or Lagrangian dispersion models are used at regional and local scales, respectively, for the calculation of the behavior of the pollutants in the atmosphere. The combination of in situ measurements and model calculations allow more accurate air quality mapping and forecasting of the pollutant concentrations as performed by the French national forecasting system PREV'AIR ([Rouil et al., 2009](#); [Malherbe and Ung, 2009](#); [Beauchamp et al., 2016](#)). However, the high cost associated with the setting-up and operation of a station network makes it necessary to limit the number of stations that can be installed and maintained in a given region. This is a significant limitation to improve the forecasting system.

In the last decade, the technological progress has opened ways to overcome this constraint by the development of miniaturized and low-cost sensors (hereafter LCS) to measure pollutant concentrations ([Kumar et al., 2015](#)). Many projects of crowdsourcing and citizen science are coming up. In Europe, fablabs are created to bring together citizens for a common purpose to measure pollution in their environment (AirCitizen, <http://aircitizen.org/>, Mobicit'Air, <http://www.mobicitair.fr/>, Ambassad'Air, <http://www.wiki-rennes.fr/Ambassad'Air>, Luftdaten, <https://luftdaten.info/>). In addition, measurement campaigns are conducted to assess the potential of these devices by installing fixed sensors (on top of buildings, on street lights, or on reference stations) and/or mobile sensors (on top of cars, bikes, or carried by citizens) offering higher spatial coverage than reference stations.

The large amount of collected information offers new opportunities of developments in air quality modelling and mapping at urban scale that are the scope of recent studies. Because low-cost sensors suffer from metrological weaknesses, a calibration is first generally applied to the raw data. Especially, linear/multilinear regression and supervised learning techniques have been developed to correct sensor measurements ([Spinelle et al., 2015, 2017](#), [Maag et al., 2015](#)). Once calibrated, LCS data are then used for air quality mapping. Statistical methodologies are broadly applied to include mobile sensor observations to produce maps of pollutants. The Land Use Regression models (LUR) have been applied in many works ([Jerrett et al., 2005](#); [Ryan et al., 2007](#); [Hoek et al., 2008](#); [Minet et al., 2018](#); [Xie et al., 2017](#)). These approaches consider the influence of the land use and the environmental features of the surrounding area to estimate the pollution. This is based on the construction of a multiple linear regression with explanatory variables (population density, distance from the road, altitude etc.). Recently, [Hankey et al., 2015](#), provided an estimate of PM_{2.5} concentrations in Minneapolis (USA) by testing 1224 different LUR using mobile measurements. Their results show that the LUR performance is dependent on the choice of the variables and most importantly on the amount of data and the frequency of the measurements. Although the results are convincing, the main limitation of the LUR methods remains the exclusion of the spatial dependence of the residuals. Other methods, such as machine learning techniques (Support Vector Regression, Decision Tree Regression, Random Forest Regression or Extreme Gradient Boosting) are used for mapping ([Muller et al., 2016](#); [Hu et al., 2017](#)). Their results demonstrate below-average performance and highlight the necessity to include meteorological parameters in the estimation. Moreover, geostatistical approaches have been applied based on low-cost sensor data. [Alvear et al., 2016](#), estimated an ozone map in Valencia (Spain) by using ordinary kriging with mobile sensor observations. The estimation shows large spots of high and low concentrations

of ozone, so the map accuracy could be improved. A more sophisticated geostatistical approach was used by [Schneider et al., 2017](#) to estimate NO₂ concentrations in Oslo (Norway). They applied external drift kriging (also called data fusion) that allows to combine fixed sensor observations and dispersion model calculations to estimate the pollutant levels at the urban scale. Data fusion is of great interest compared to other approaches. Unlike exclusively statistical techniques, external drift kriging allows to consider the spatial variability of the process to be interpolated. Although it does not account for discontinuities in spatial correlations due to street canyon effects at the local scale, it offers a straight forward implementation because the dispersion model outputs are used without any change in the model formulation. By applying this approach, Schneider et al. found that data fusion can produce realistic hourly concentration fields of NO₂ and the performance of the approach is dependent on the number of observations, their spatial distribution, the uncertainty of the measurements and the model capability to reproduce urban air quality patterns. They provided the first data fusion results using low-cost sensor data. However, they did not consider the sensor measurement uncertainty in their estimation and they did not include mobile sensor measurements.

In this paper, data fusion is performed in Nantes (France) using fixed and mobile low-cost sensor observations of PM₁₀. The feasibility and the potential added-value with respect to the dispersion model (ADMS-Urban) calculations of using fixed and mobile low-cost sensor observations for air quality mapping via an external drift kriging approach is investigated. The observations that are used in the data fusion are presented in [Section 2](#), the preprocessing which is applied to the raw dataset of the LCS measurements is detailed in [Section 3](#), the data fusion technique is described in [Section 4](#), the results are presented and discussed in [Section 5](#), followed by the conclusions.

2. Observations

AtmoTrack (<https://atmotrack.fr>), a French company created in 2015 in Nantes, provided the sensor data. AtmoTrack participated in the Airlab 2018 challenge (<http://www.airlab.solutions/en/discover>). They showed that AtmoTrack sensors that measured PM are satisfactory compared to other existing sensor systems (Airlab, 2018) by assigning a rating for their accuracy of 7/10 based on the Sensor Evaluation Toolbox (SET, [Fishbain et al., 2017](#)). They also obtained a patent for the mobile sensor design (<https://bases-brevets.inpi.fr/fr/document/FR3073942.html?s=1590659615382&p=5&cHash=7a962d67878558c00956ee2f102afbc>) and they demonstrated that up to 50 km/h the sensor motion does not affect the measurement. Further, beyond 80 km/h the data is no longer considered. AtmoTrack has deployed fixed and mobile low-cost sensors that provide PM₁₀ and PM_{2.5} concentrations in urban areas to build a database for a better estimation of outdoor air quality.

This work focused on the estimation of the PM₁₀ concentrations using the AtmoTrack low-cost sensor observations in Nantes in November 2018. The reference station measurements ([Fig. 1a](#)) were provided by Air Pays de La Loire (hereafter AirPDL, <http://www.airpl.org/>) with a 15-min time resolution. Note that the station measurements are not used in the spatial interpolation but only in the sensor data preprocessing as presented in section 3. During the sampling period, AtmoTrack deployed 16 fixed sensors ([Fig. 1b](#)) including 3 replicates at Victor Hugo station (station under the traffic influence) and 3 other replicates at La Bouteillerie station (station under urban background influence). Most of the fixed sensors are in the city center excepted the sensor with the ID 10, which is in the west part of the city. In addition, 19 mobile sensors were on-board of driving school cars, ambulances and service vehicles to measure PM₁₀ concentrations over numerous routes each day of the sampling period. The routes are presented for each sensor in [Fig. 1c](#). The vehicle routes ensure a unique spatial coverage over the urban area although they rely on their itineraries and on their drive time (mainly daytime). [Fig. 1d](#) shows that the

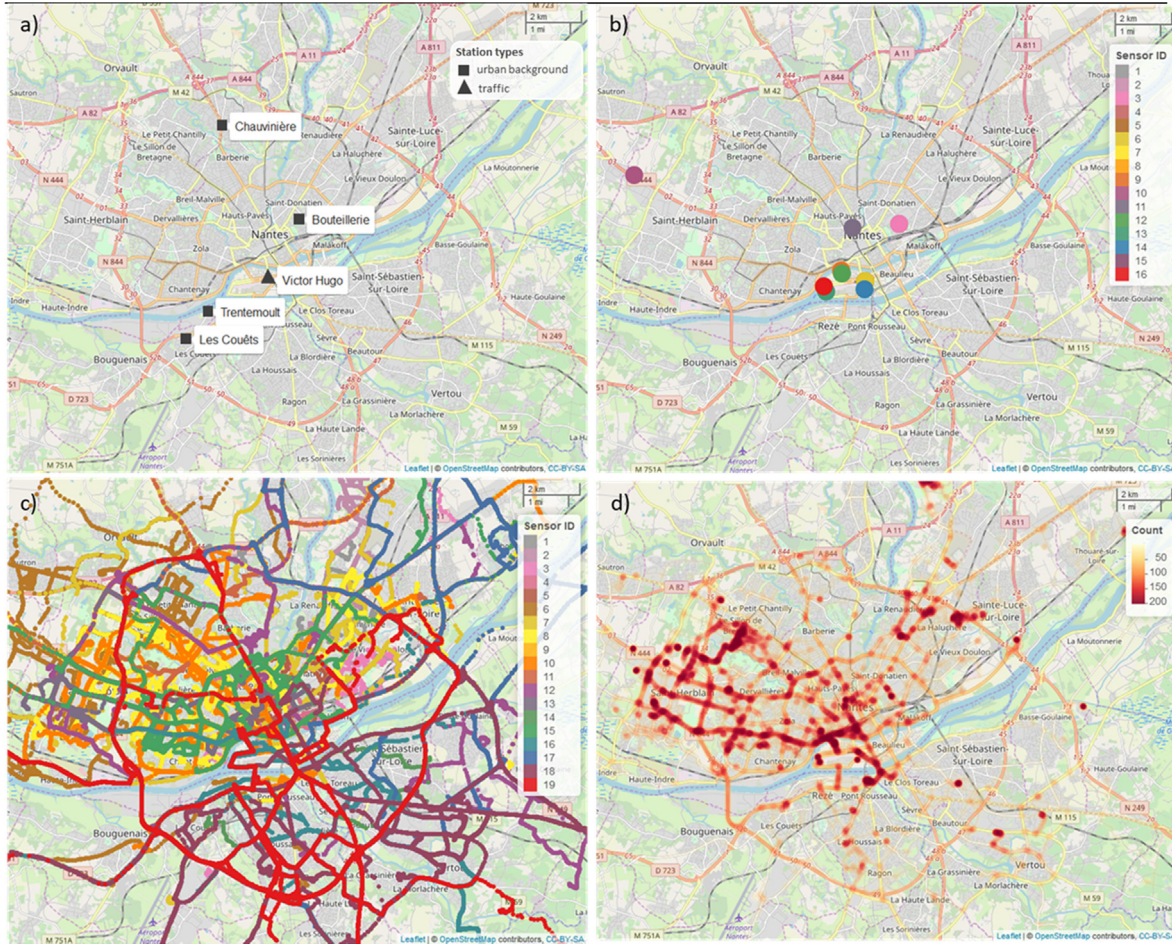


Fig. 1. The reference monitoring stations (Air Pays de la Loire network) (a), the fixed LCS positions (b), the sampling routes of the mobile LCS (c) and the heatmap of the fixed and mobile LCS observations (d), are given for November 2018 in Nantes.

locations with the largest number of observations are mainly in the center and the north west part of the city.

The reference station measurements, the raw fixed and mobile LCS observations have been compared over the sampling period. The fixed sensor observations were aggregated in time (15 min average) to match the time resolution of the reference measurements. The comparisons of the two datasets at Victor Hugo (Fig. 2a) and La Bouteillerie (Fig. 2b) show that the fixed sensor distribution of PM_{10} concentrations is characterized by two modes whereas there is only one mode in the reference observations. The first mode is between 0 and 10 $\mu\text{g}/\text{m}^3$ and might be explained by a poor detection of ultra-fine particles by the devices. The second mode, between 30 and 40 $\mu\text{g}/\text{m}^3$, corresponds most likely to the real concentrations of PM_{10} with a shift toward higher values. This might be due to a granulometry effect related to the measurement technique. These hypotheses should be investigated in a specific work and they are not the scope of this study. Fig. 2c shows the distributions of the fixed and mobile sensor PM_{10} observations with the initial time resolution (10 s) and the reference observation distribution. As expected, the distributions of mobile and fixed sensor observations are consistent because of the two similar modes unlike reference stations. In addition, the density of the sampling time (Fig. 2d) is comparable between the fixed LCS and the reference stations. That demonstrates the smooth operation of the devices. Mobile sensors are showing gaps in the sampling time. The maximum density of measurements is observed at the end of the sampling period. In addition, there is a decrease in the number of measurements at the end of each week. There are fewer observations from mobile sensors during weekends and especially on Sundays because sensors are installed on service

vehicles and driving-school cars.

To assess the consistency over time of the PM_{10} observations, the average of the 3 fixed LCS replicate observations have been aggregated to a 15-min time resolution and compared to the reference measurements at Victor Hugo (Fig. 3a) and at La Bouteillerie (Fig. 3b) stations. For the entire sampling period, the average of the LCS observations are consistent with the reference station observations. However, LCS overestimate the PM_{10} concentrations (up to 30 $\mu\text{g}/\text{m}^3$ between November 15th and November 23rd at both stations). Some small variations (up to 20 $\mu\text{g}/\text{m}^3$ between November 8th and November 13th) recorded by the stations are not seen by the fixed devices. These measurement differences could be explained by the effect of the detection limit of the instruments. Also, a high pollution event is recorded at Victor Hugo on November 27th that is not seen by the LCS replicates. A device malfunction or the positioning of the sensors relative to the station could be an explanation for this failure. In fact, the impact of the instrument features on the measurements should be further investigated in a dedicated study and this is not the scope of this paper. In addition, sporadic pollution events are only measured by the LCS (November 15th at Victor Hugo). As there is no reason for the reference station not to record the right pollutant levels it seems that these events could be associated to malfunction of the devices. The correlation coefficient between the reference measurements and the LCS (Fig. 3, right panels) is satisfactory for both stations. However, the correlation is higher at La Bouteillerie ($R = 0.85$) than at Victor Hugo ($R = 0.62$). The very local emissions of PM_{10} (due to traffic and other human activities) at Victor Hugo could be an additional complication for sensor measurements.

To reduce as much as possible the bias related to the low-cost sensor

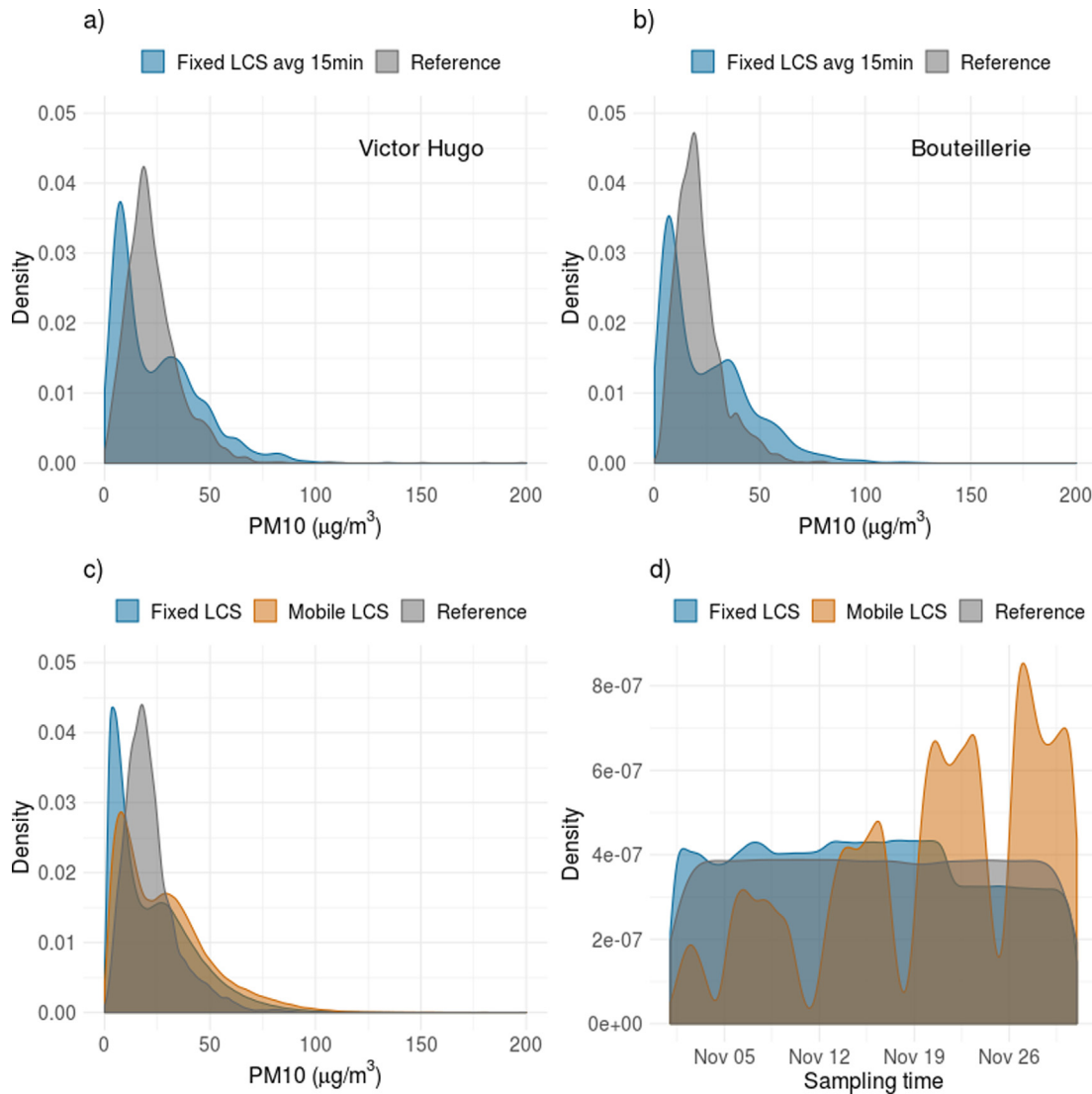


Fig. 2. The entire dataset in November 2018 in Nantes is presented as: the distributions of the co-located observations at Victor Hugo of the reference (in grey) and the fixed LCS (in blue) at 15-min time resolution are in panel (a), the distributions of the co-located observations at La Bouteillerie of the reference (in grey) and the fixed LCS (in blue) at 15-min time resolution are in panel (b), the distribution of all observations of the reference stations at 15-min time resolution (in grey), the fixed (in blue) and mobile (in orange) LCS at 10 s time resolution are in panel (c), and the density of the sampling time of the stations, and fixed and mobile LCS are in panel (d).

measurements to be used in the mapping approach, a preprocessing on LCS data has been applied as discussed in section 3.

3. Preprocessing

AtmoTrack sensors were placed next to the Air Pays de la Loire reference stations to be pre-calibrated before being installed on vehicles. No adjustment was made after the sensors were deployed. The preprocessing of the LCS raw dataset proposed in this work consists of two steps. The first step is the elimination of unreliable data based on the repeatability criterion. The second step is the correction of the daily variation of the background concentrations.

The concentration threshold based on the repeatability criterion is calculated according to Spinelle et al. (2013). Their approach is based on laboratory tests for gaseous pollutants, however because there is no reference that defines the repeatability for PM ambient air measurement, this method was adapted.

LCS observations which are below this threshold are then removed from the dataset. Especially, a period without pollution (very low PM₁₀ concentrations for a period of 30 min at least) is identified from the

reference station observations (Victor Hugo station). Then, the LCS (fixed sensors installed at the station) observations corresponding to this period are selected. From this selection of data, the standard deviation is derived as described by Eq. (1).

$$S_x = \sqrt{\frac{\sum_{i=1}^N (x_i - \bar{x})^2}{N - 1}} \quad (1)$$

With x_i the individual measurement, \bar{x} the mean response of the sensor, and N the number of measurements. Then, the repeatability threshold (R_p) is calculated such as presented in Eq. (2).

$$R_p = 2\sqrt{2S_x} \quad (2)$$

PM₁₀ and PM_{2.5} concentrations from LCS measurements are closely related. AtmoTrack estimates the PM_{2.5} concentrations from the raw measurement then PM₁₀ concentrations are calculated on the PM_{2.5} basis as it is detailed in the supplementary material document as S1. Therefore, we consider both PM categories for this first step of the preprocessing. R_p is 4 $\mu\text{g}/\text{m}^3$ for PM₁₀ and 2 $\mu\text{g}/\text{m}^3$ for PM_{2.5}. Both thresholds are applied to the dataset. Note that the repeatability

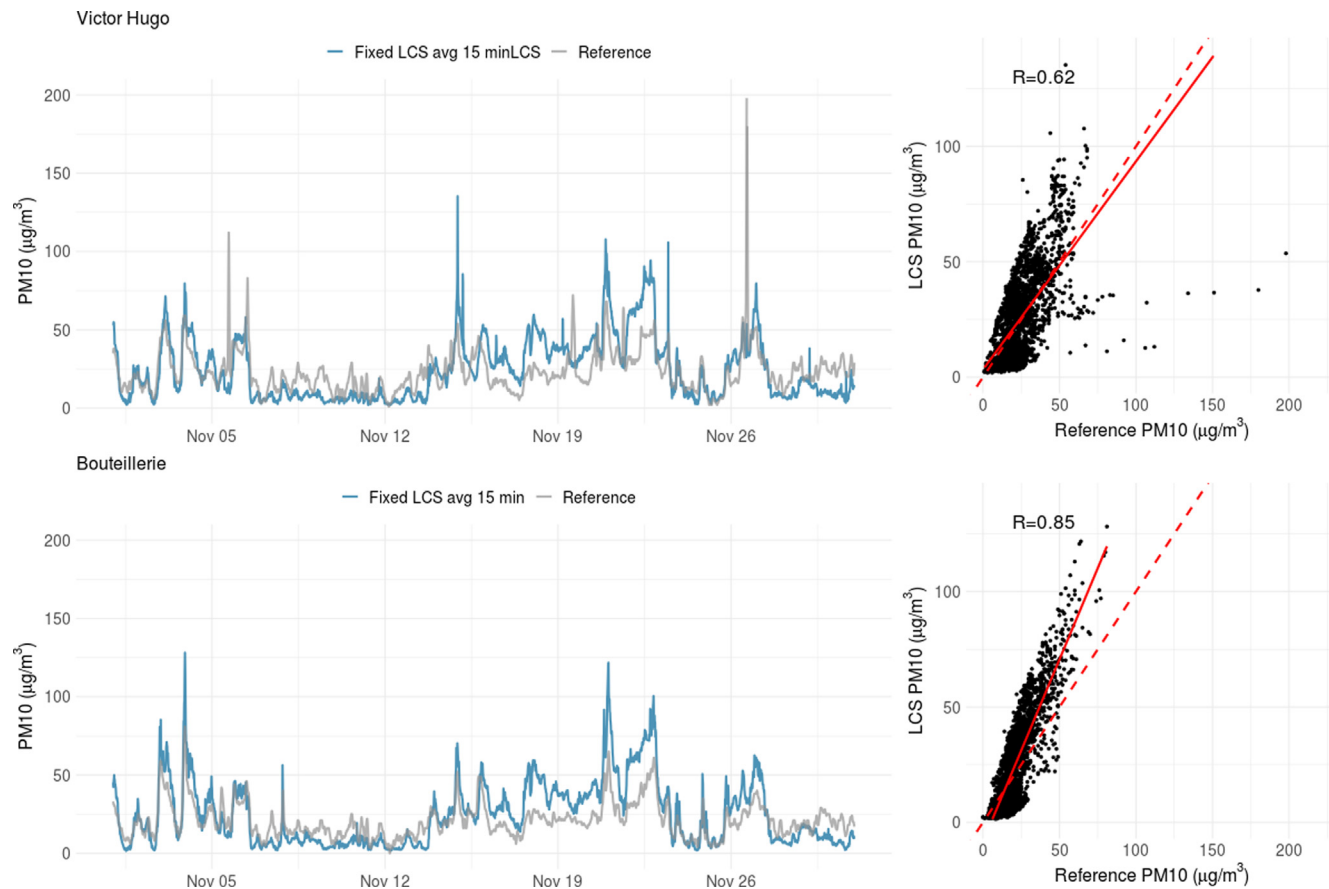


Fig. 3. Timeseries of the PM₁₀ observations in $\mu\text{g}/\text{m}^3$ (left panels) from the average of 3 fixed LCS (in blue) and the reference station (in grey) at Victor Hugo (upper panel) and La Bouteillerie (bottom panel), and the corresponding correlation plots (right panels).

criterion is calculated using the fixed LCS data because the comparison with the reference station is necessary. The repeatability threshold based on fixed data is then applied to the mobile observations. Indeed, because of the spatial and temporal representativity issues illustrated by Figs. 1d and 2d, the repeatability can't be estimated using mobile observations. This could imply a bias on the mobile data filtering. Considering PM_{2.5} and PM₁₀ for the entire dataset, we obtained a 6.5% removal of mobile LCS data and a 14% removal of fixed LCS data. PM concentrations measured on road by mobile LCS are higher in average than those measured by fixed LCS installed close to the stations. Therefore, less data with low PM concentration values is eliminated from the dataset from mobile LCS data.

Once the thresholding step is complete, the correction of the daily variation of the background (Hankey et al., 2015) is applied. The corrected concentration is determined from Eq. (3).

$$C_r = C_i - (B_{g,LCS} - B_{g,stations}) \quad (3)$$

With C_r the corrected concentration value, C_i the initial concentration value, $B_{g,LCS}$ is the background calculated from all the LCS measurements and $B_{g,stations}$ the background calculated from all reference stations. $B_{g,LCS}$ corresponds to the median value in a moving-window of 15 min on a continuous run of mobile measurements. A continuous run is defined as the measurements from a mobile sensor without interruption of measurements greater than 5 min. $B_{g,stations}$ is the daily average of the reference station measurements.

The PM₁₀ observation distribution of the fixed and mobile LCS estimated by the preprocessing are presented in Fig. 4.

As presented in Fig. 2, the preprocessed fixed sensor observations have been aggregated in time to match the time resolution of the reference measurements, i.e. 15 min (Fig. 4). The comparisons of the

datasets at Victor Hugo (Fig. 4a) and La Bouteillerie (Fig. 4b) show that the two modes that characterize the distributions of the fixed LCS raw data are not present after the preprocessing. Thus, the fixed LCS and reference observation distributions are more comparable. Fig. 4c shows the distributions of the preprocessed fixed and mobile LCS observations with the initial time resolution (10 s) and the reference observation distribution from all stations. The three distributions show similar mean and dispersion implying a consistency over the estimation domain of the pollutant measurements for the 3 networks. Because of the elimination of observations from the raw dataset, the sampling time density (Fig. 4d) of the preprocessed LCS observations has been decreased especially for the fixed sensors.

To assess the accuracy of the preprocessed dataset, the hourly average of the raw and preprocessed PM₁₀ observations from mobile and fixed LCS are compared to the ADMS-Urban dispersion model calculations from 7 am to 7 pm in November 2018. ADMS-Urban is a modeling platform which is developed by the Cambridge Environmental Research Consultant (CERC; Carruthers et al., 1997). It includes several models for the calculation of the pollutant concentrations at the urban scale. It allows to perform calculation from the local scale to the city scale and this is a reference system for the assessment of the population exposure to air pollution sources. AirPDL uses ADMS-Urban for their forecasts of pollutant concentrations at the urban scale and they provided the simulation results. The use of ADMS-Urban is supported by a continuous validation (<https://www.cerc.co.uk/environmental-software/model-validation.html>) and comparison studies (Malherbe et al., 2010; Tognet et al., 2015, 2016). The model allows a Gaussian dispersion of the pollutants and includes a street canyon formulation. ADMS-Urban outputs which are used in this study are from an automated forecasting system that runs daily for the

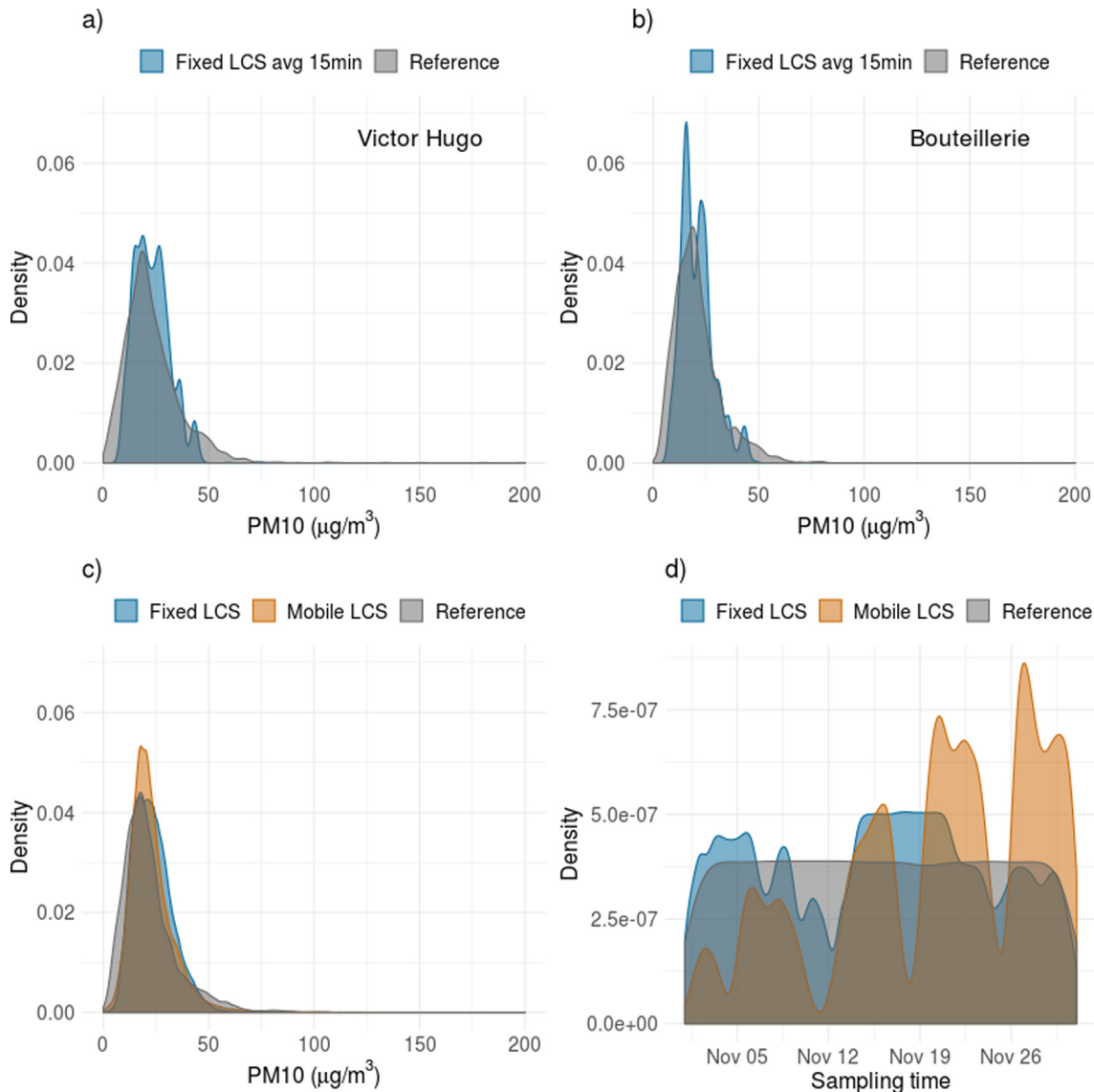


Fig. 4. The entire dataset in November 2018 in Nantes is presented as: the distributions of the co-located observations at Victor Hugo of the reference (in grey) and the fixed LCS (in blue) at 15-min time resolution are in panel (a), the distributions of the co-located observations at La Bouteillerie of the reference (in grey) and the fixed LCS (in blue) at 15-min time resolution are in panel (b), the distribution of all observations of the reference stations at 15-min time resolution (in grey), the fixed (in blue) and mobile (in orange) LCS at 10 s time resolution are in panel (c), and the density of the sampling time of the stations and fixed and mobile LCS are in panel (d).

previous and next few days. The background pollution is calculated on average over a set of grid points of a large-scale model (ESMERALDA, <http://www.esmeralda-web.fr/>, or PREV'AIR, <http://www2.prevair.org/>) and it is validated daily by AirPDL. Hourly model outputs are considered as the true state and give information at locations without measurement from the reference station network. To make the comparison, at each measurement position, all measurements occurring during an hour are averaged. Then, the nearest model grid point to the observation position is selected to be compared. Note that model grid points are clustered over the main highways (6 m spatial resolution) and far from the roads the grid becomes regular (250 m spatial resolution). The analysis of the hourly average shows that raw data overestimate by up to $4 \mu\text{g}/\text{m}^3$ at 10 am (*underestimate by up to $8.5 \mu\text{g}/\text{m}^3$ at 5 pm*) the model before (*after*) 11 am. The preprocessing allows to reduce the difference (decrease of up to $5.5 \mu\text{g}/\text{m}^3$ at 5 pm) with the model calculations (Fig. 5a). In addition, the PM₁₀ concentration distributions of the preprocessed LCS data are more in agreement with the model output distributions unlike the raw LCS data (Fig. 5b).

These results demonstrate the relevance of applying a preprocessing on LCS raw data. We are then more confident in using sensor observations for air quality mapping. The approach used in this work to estimate the PM₁₀ concentrations in Nantes is the data fusion. This is described in the following section.

4. Data fusion: method

Data fusion allows to combine different sources of information also called auxiliary variables to estimate a map of pollutant concentrations. This is based on universal kriging, a geostatistical method. Kriging is an approach broadly used for air quality mapping at the regional and urban scale (Liu et al., 1996; Ferreira et al., 2000; Jerret et al., 2001; Künzli et al., 2005; Malherbe et al., 2005; Beauchamp et al., 2010, 2014, 2017, 2018; Xie et al., 2017). Kriging aims to estimate the value of a random variable (random process which describes the observations) at locations of a spatial field, based on the measurements. The main concept of kriging is that the measuring points that are close to

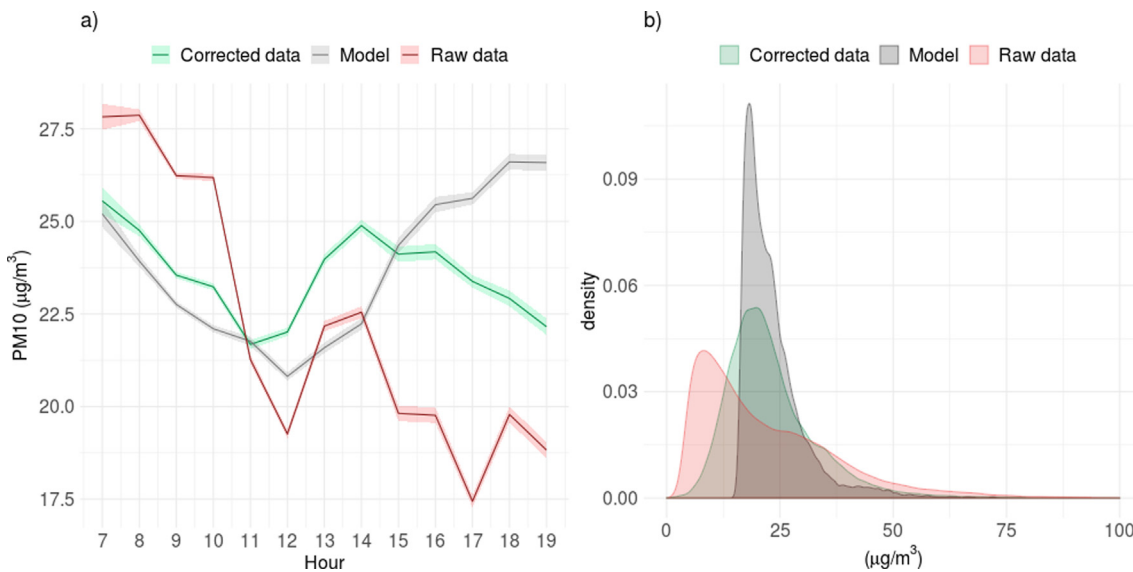


Fig. 5. The hourly comparison of the raw data (in red), the corrected data (in green), and the model (ADMS-Urban, in grey) has been performed in November 2018 as shown by the timeseries (a) and the density plots (b). In panel (a), the shaded areas correspond to the variability in the vicinity of the model point, i.e., the mean \pm the standard deviation.

the estimation point should have a higher weight in the estimation than the distant measuring points. This is based on a good knowledge of the spatial structure of the domain which is represented by the variogram or co-variogram (second order properties) of a random function (Goovaerts, 1997; Wackernagel, 2003; Chiles and Delfiner, 2012; Lichternstern, 2013). Kriging involves deriving linear combination of the data which ensures the minimal estimation variance under a non-bias condition. At a point s_0 , the concentration estimate $\widehat{y(s_0)}$ is given by Eq. (4).

$$\widehat{y(s_0)} = \sum_{i=1}^N \lambda_i y(s_i) \quad (4)$$

Where $y(s_i)$, $i = 1\dots N$, are the observed concentrations at sampling locations through the entire domain (unique neighborhood) or within a limited neighborhood of s_0 (moving neighborhood), and λ_i , $i = 1\dots N$, are the kriging weights.

The variogram allows to derive the variance of the estimation error (kriging variance) which gives the location where the error is relatively high or low. The strength of the kriging approach is to give an information on the error and on the uncertainty of the estimated map. Among the kriging methods, the universal kriging allows to consider additional information to make estimate more accurate. Universal kriging, more specifically external drift kriging, is based on a linear regression with auxiliary variables and a spatial correlation of the residuals and allows to combine simultaneously observations and additional information. Hereafter, this kriging approach is called data fusion. The main hypothesis is that the global mean is not constant through the domain and it relies on explanatory variables. This kriging technique has been used for several years in the monitoring air quality system for spatial interpolation at urban scale (Beauchamp et al., 2016) and at the regional scale (PREV'AIR, Malherbe and Ung, 2009). The novelty in this work is the use of fixed and mobile low-cost sensor data to perform data fusion.

For $y(s_0)$, which is the pollutant concentration to be estimated at a location s_0 , the hypothesis is a linear relation between $y(s_0)$ and the considered auxiliary variables as explained by equation (5) and (6).

$$y(s_0) = m(s_0) + \varepsilon(s_0) \quad (5)$$

$$m(s_0) = b_0 + b_1 x_1(s_0) + b_2 x_2(s_0) + \dots + b_p x_p(s_0) \quad (6)$$

Where $m(s_0)$ is the drift of the mean, b_0, b_1, \dots, b_p are the coefficients

of the linear regression, and x_0, x_1, \dots, x_p , are the auxiliary variables. ε corresponds to the stationary random process which is associated with a semi-variogram. In addition, the kriging weights must satisfy the drift condition described in Eq. (7).

$$\forall x_p: x_p(s_0) = \sum_{i=1}^N \lambda_i x_p(s_i) \quad (7)$$

In this work, the spatial drift of the mean is described by the 2016 annual average concentrations of the pollutant simulated by the ADMS-Urban dispersion model provided by AirPDL (Fig. 6). The modeled annual average is representative of the main patterns of the pollutant concentrations and it was interpolated over the modelling domain by AirPDL. The hourly model outputs for November 2018 were provided at grid points. We assessed the feasibility to use them as external drift in kriging. We interpolated the hourly outputs and calculated the correlation with sensor observations. Results did not show better correlation than using the annual average. Thus, to avoid additional bias by interpolating ADMS-Urban hourly outputs, we defined the annual average as the drift. This variable is displayed in Fig. 6 for the estimation

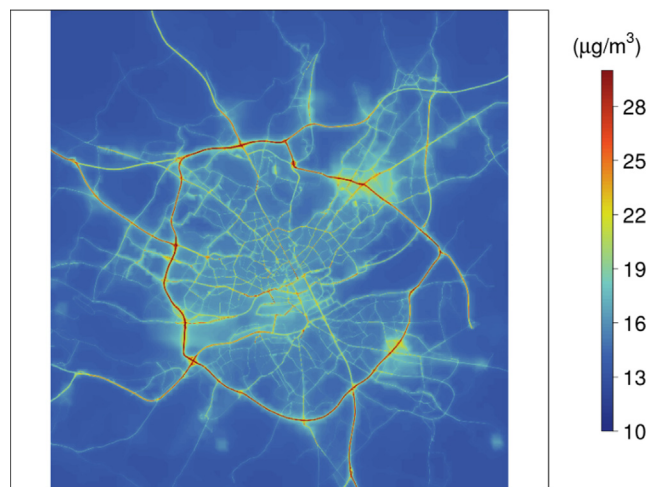


Fig. 6. The annual average of PM₁₀ concentrations (in $\mu\text{g}/\text{m}^3$) for the year 2016 calculated by ADMS-Urban (provided by Air Pays de la Loire) in Nantes and used as the drift in the kriging approach.

domain which corresponds to Nantes and its surroundings.

To consider the measurement uncertainty and the variability of the LCS data in the kriging, the variance of measurement errors (hereafter VME) is defined as an input of the calculation (the VME of each sample data is added to the corresponding diagonal term of the covariance matrix before solving the kriging system). Especially, the VME is the combination of i) the dispersion of the pollutant concentrations observed at a position over the estimation period (an hour in this work), versus the number of observations at this position and ii) the measurement uncertainty (Macé et al., 2010). The VME calculation is given in Eq. (8).

$$VME_i = \left[\left(\frac{\sigma}{\sqrt{N}} \right)^2 + \frac{\nu_r^2}{N} \sum_{j=2}^N (C_j)^2 \right]_i \quad (8)$$

Where σ is the standard deviation of the pollutant observations at the position i , N is the number of observations at the position i , ν_r is the constant relative type uncertainty (which depends on the type of sensor), and C_j is the j^{th} pollutant concentration at the position i .

The accurate estimation of the measurement uncertainty is challenging. In this study, a relative uncertainty is considered based on the definition of the 3 networks of measurements. These networks, i.e. the reference stations, the fixed and the mobile LCS, are characterized by the number of observation locations, their measurement accuracy and the mobility. The first network, which consists of the reference stations, is very sparse but the quality of the observations is high with a maximum uncertainty of 25% meeting the requirements of the European directive (directive 2008/50/CE and 2004/107/CE). The second network, which corresponds to the fixed sensors, allows to add many measurement locations but with higher uncertainty. The third network, which corresponds to the mobile sensors, offers an unequalled high spatial coverage but implies issues of measurement (mainly spatial and temporal representativeness, and heterogeneity of the data) and a high uncertainty. In this study, the uncertainty definition relies on the LCS observations analysis and the European directives requirements. In the following, a maximum of 50% of uncertainty is considered for the fixed LCS and 75% for the mobile LCS. After all, the VME allows to allocate more weight to the data points characterized by low uncertainty and variability in the estimation of PM_{10} concentrations.

Note that kriging is performed by way of a R computing language code that uses the RGeostats package (a package for geostatistical applications, MINES ParisTech / ARMINES (2019), RGeostats: The Geostatistical R Package. Version: 11.2.3, Free download from: <http://cg.ensmp.fr/rgeostats>). The data fusion results are presented in the following section.

5. Data fusion results

Because this is computationally expensive to apply the data fusion with a large amount of observations, we performed the estimation on 11/29/2018. This day is one of the most sampled in November 2018 with more than 15,000 observations and it does not show any unexplained variations of PM_{10} concentrations. The hourly PM_{10} map is estimated using the fixed and mobile LCS observations collected during each hour. Thus, at each measurement position, the average of the observations is considered, and the external drift kriging approach is applied.

5.1. Estimation of hourly PM_{10} concentrations in Nantes

To illustrate the data fusion in detail, results are first presented at 9 am on 11/29/2018. Fig. 7a shows the drift on the background characterized by PM_{10} concentration maximums on the roads (up to $48.5 \mu g/m^3$). Far from the main roads, the PM_{10} levels are about $12.5 \mu g/m^3$. The LCS observations are mainly located in the center and the east (from the south to the north) of the city with concentration

levels ranging from 12 to $64 \mu g/m^3$. The corresponding VME is presented in Fig. 7b. The minimum VME is associated with the fixed LCS observations ($72 (\mu g/m^3)^2$) whereas the highest VME is calculated for the mobile LCS data points and depending on the location it can reach $1467 (\mu g/m^3)^2$. For these data points, the high VME is explained by the high measurement uncertainty (75%) and especially a high variability meaning that the dispersion of the observations at these points during the hour is significant.

Note that the reference station measurements are not used in the kriging approach because the data preprocessing is based on these observations (cf. Section 3).

The fused map and the kriging standard deviation are given in Fig. 7c and d, respectively. They are both reliant on the correlation between the drift and the LCS data (Fig. 8a), and on the calculation of the variogram of the residuals (Fig. 8b). The correlation is calculated by considering the nearest model output point grid to the data point. In this case, the correlation (Fig. 8a) is weak with $R = 0.18$. This may be mainly due to the high variability of the sensor measurements implying important differences with the drift patterns. In addition, the choice of the 2016 annual average of the modeled pollutant concentrations does not allow to capture local pollution events which might be observed by the sensors. As mentioned in section 4, the correlation between sensor data and hourly model outputs was investigated but the results were not conclusive and further testing is needed before using such outputs. Sensitivity tests were conducted to determine whether considering a buffer of the model outputs (defined by a radius from 10 m to 500 m) around the LCS observation instead of the nearest point could improve the correlation between the drift and the LCS observations. However, these tests did not show significant improvement. Details on the results of the sensitivity tests can be found in the supplementary material document as S2. The quality of the correlation has a significant impact on the data fusion because the drift must provide a statistical explanation of the observations. The better the correlation, the better the linear regression in kriging. The residuals between the drift and the LCS data are calculated still considering the nearest model output point grid to the data position. Then the variogram of the residuals is determined (Fig. 8b), given the variance of the residuals in space over the domain. Data fusion is performed based on this information. As a result, at 9 am the fused map shows that PM_{10} concentrations range from 19.9 to $30.5 \mu g/m^3$. The maximums of concentrations are on the roads similarly to the drift. The average PM_{10} concentrations over the domain calculated by the data fusion is 1.5 times higher than the drift (20.6 and $13.7 \mu g/m^3$, respectively). The annual mean may underestimate the potential pollution occurring at hourly resolution. At 9 am, the average PM_{10} concentrations of the reference stations is higher than the annual mean over the domain ($16 \mu g/m^3$), so the pollutant concentrations are raised to a level which is representative of this specific time with a greater or lesser magnitude depending on sensor observations. Most of the LCS data points are characterized by a high VME. Thus, only the fixed sensor data and a few mobile sensor data points have a significant influence in the data fusion. The concentrations associated with the low VME data points are then weighted for the estimation. Consequently, the kriging standard deviation shows smaller errors ($5 \mu g/m^3$, refer to Fig. 7d) around locations where there are high weighted LCS observations. Higher errors (up to $8 \mu g/m^3$, refer to Fig. 7d) are remarkable far from the observations.

To summarize the results for the entire day (11/29/2018), the hourly fused maps of PM_{10} concentrations are presented from 7 am to 7 pm in Fig. 9. Disparate responses to the external drift kriging approach are remarkable such as:

- At 8 am, 11 am, 0 pm, 1 pm, 2 pm, 3 pm and 4 pm, there are local hotspots of high or low PM_{10} concentrations. Those are associated with a few LCS data points of high or low PM_{10} concentrations with a relatively high influence in the data fusion (the hourly average of the data points used in kriging is given in the supplementary

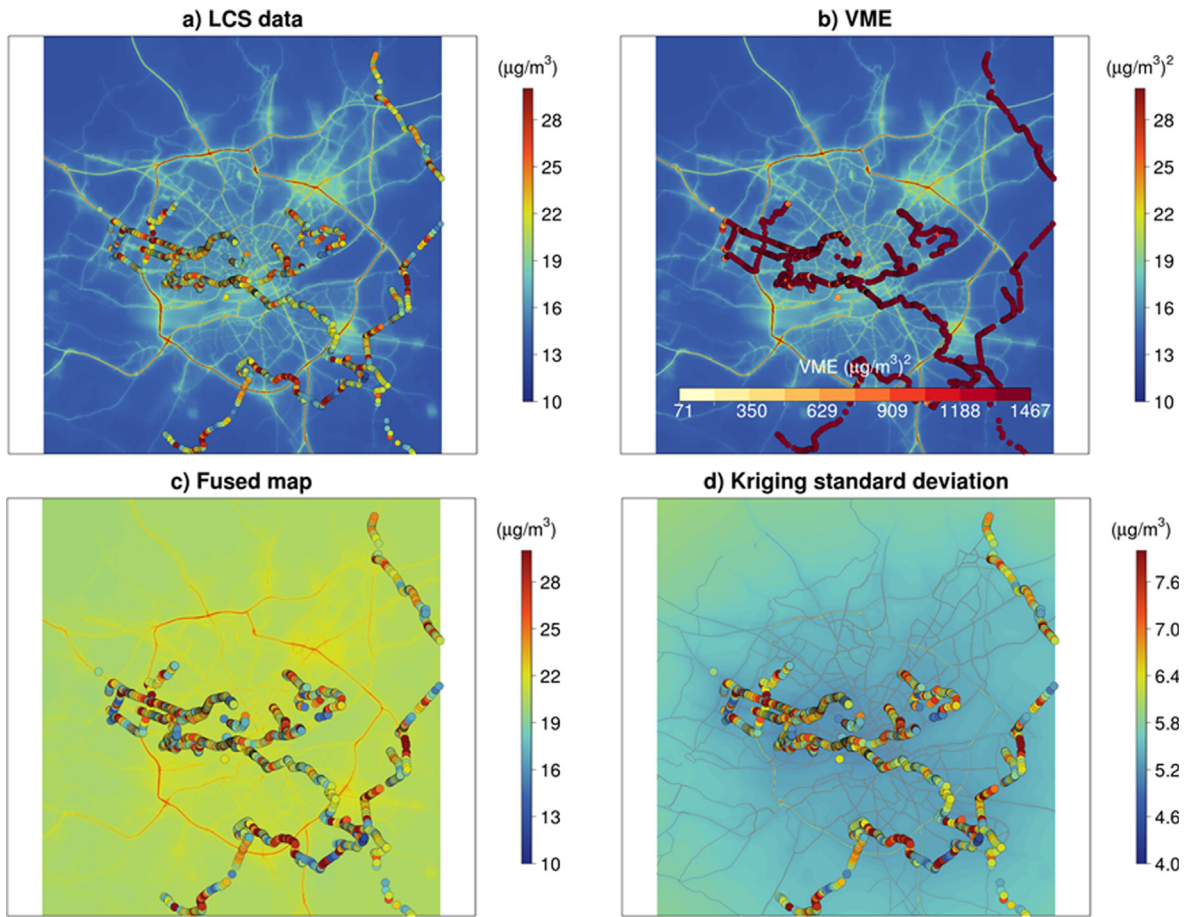
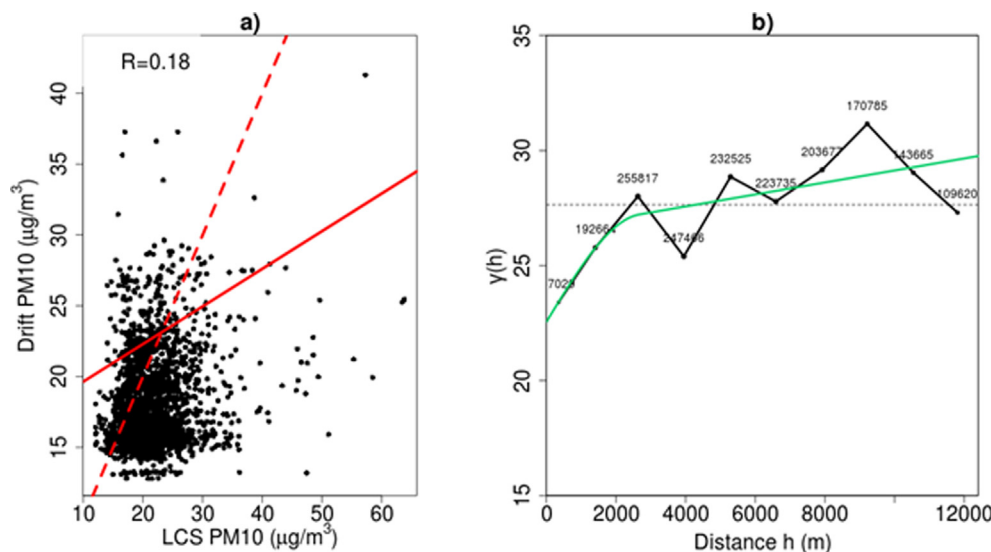


Fig. 7. The PM₁₀ LCS observations (in $\mu\text{g}/\text{m}^3$) overlaid the 2016 annual average of the PM₁₀ concentrations (in $\mu\text{g}/\text{m}^3$) calculated by the ADMS-Urban model that is defined as the drift in the data fusion (a), the variance of the measurement error (VME, in $\mu\text{g}/\text{m}^3$)² is shown with the drift in the background (b), the hourly fused map with the PM₁₀ LCS observations (c) and the kriging standard deviation with the PM₁₀ LCS observations and the shapefile of the main roads on the background (d), are presented on 11/29/2018 at 9 am in Nantes.



materials as S3). This means that these points are associated with a relatively low VME in kriging. The hourly VME associated with the fused maps is given in the supplementary materials (S4). As expected, the fixed sensor data points are characterized by the lower VME at any time. Depending on the hour, some mobile sensor data points are also characterized by low VME and are considered as

reliable data in kriging. Where there is no LCS observation, the background is updated depending on the LCS data with the most important weight by increasing or decreasing the baseline concentrations defined by the drift. In addition, for those hours, the correlation between the LCS data and the drift is ranging from 0.01 to 0.18 and the variograms of the residuals show high nugget effect

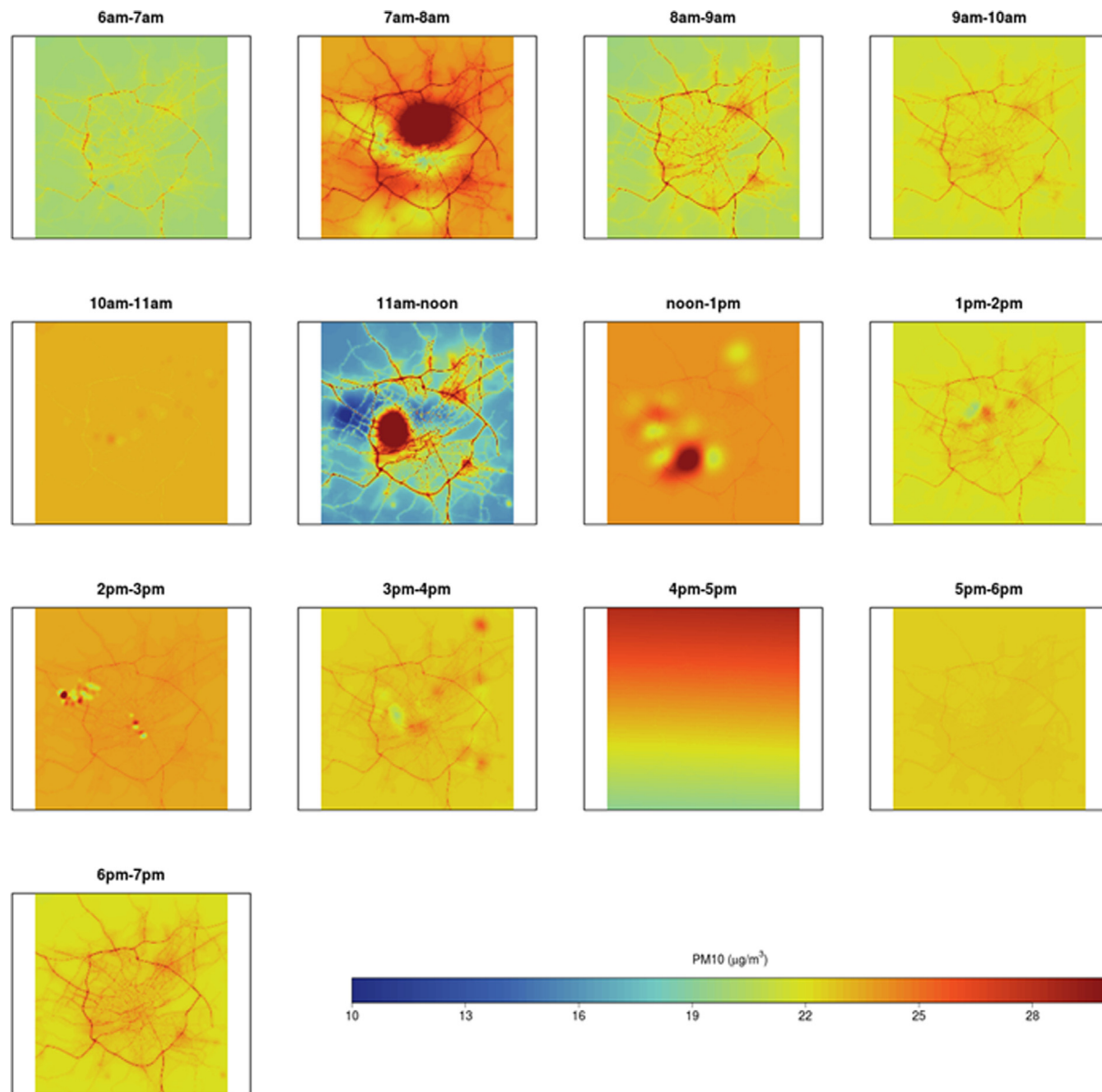


Fig. 9. The fused maps for PM_{10} derived from the external drift kriging approach are shown from 7 am to 7 pm on 11/29/2018 in Nantes.

($20 \mu\text{g}/\text{m}^3$) which supports the partial absence of correlation between LCS data and drift (cf. supplementary materials S5 and S6). This implies a relatively high kriging standard deviation, up to $12 \mu\text{g}/\text{m}^3$ (cf. supplementary materials S7).

- At 7 am, 9 am, and 10 am, there is no remarkable hotspots of PM_{10} concentrations. For these hours, there are more data points associated with low VME that influence data fusion. The correlation between the LCS data points and the drift is ranging from 0.05 to 0.28. The variogram of the residuals is characterized by a high nugget effect ($20 \mu\text{g}/\text{m}^3$) but it is better structured and a variogram model can be more easily fitted. This implies a relatively lower kriging standard deviation, up to $6 \mu\text{g}/\text{m}^3$ (cf. supplementary materials S7).
- At 5 pm, 6 pm and 7 pm, the correlation between the data and the drift is negative. Thus, the drift for those hours is not a sufficient approximation to be used for data fusion. Consequently, the estimations are admitted as no relevant.

Results presented in Fig. 9 demonstrate that depending on the number and the position of data points that show a low VME, the LCS

data may have a varying impact in the estimation. In addition, the correlation between the data and the drift, and the related variogram on residuals are responsible for the high estimation error. The main issue remains on the fact that LCS measurements are not well statistically explained by the drift. This could be due to the potential remaining bias associated with the LCS data which has not been corrected by the preprocessing described in section 3. The average from 7 am to 7 pm, as presented in Fig. 10, is a more valuable estimation of the pollutant levels for the day. That supports the fact that including all data is important to get a useful information. The daily average is used for the assessment of the data fusion performance as discussed in the following section.

5.2. Data fusion performance

To assess the data fusion performance, first the results were compared to the model outputs and the observations of the reference stations. Then, we performed a sensitivity study by focusing on the effect of the measurement uncertainty on the estimation.

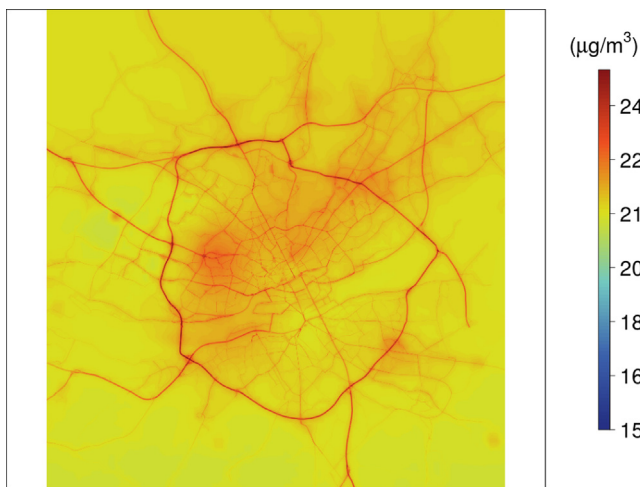


Fig. 10. The daily average fused map for PM₁₀ on 11/29/2018 in Nantes.

5.2.1. Comparison between reference observations, model and data fusion

The observations of the reference stations, the data fusion and the hourly modeled PM₁₀ concentrations were averaged over the day (from

7 am to 7 pm) as mentioned in [Section 5.1](#). The daily averages are compared ([Fig. 11](#)) at each station of the regulatory network of AirPDL ([Fig. 1a](#)). [Fig. 11](#) shows that considering the model alone implies 8% bias whereas including the LCS observations reduces the bias to 2%. However, the concentration distributions related to the data fusion are characterized by a lower dispersion than the reference observations and the model estimation (1.1 µg/m³ for data fusion compared to 5.1 µg/m³ and 3.3 µg/m³, for reference observations and model estimation, respectively). Especially, the fusion smooths the PM₁₀ peaks related to local pollution events potentially occurring near the stations. This is especially clear in the hourly comparison presented in the supplementary materials as S8. This could be explained by the predominance of the drift over the data when the related VME is high. Note that because we consider the mean of the observations at the measurement positions over the estimation period (an hour), a smoothing of the pollution events is expected for this period. In fact, local pollution events are minimized in the estimation. This is remarkable, especially at Victor Hugo station, which is under the influence of traffic. In addition, the raw LCS data were preprocessed using the observations from all the reference stations (especially the daily mean of all the reference observations was used, cf. [Section 3](#)). This way the data fusion implies a slight overestimate of the PM₁₀ concentrations at urban background stations and a slight underestimate at the traffic station compared to the

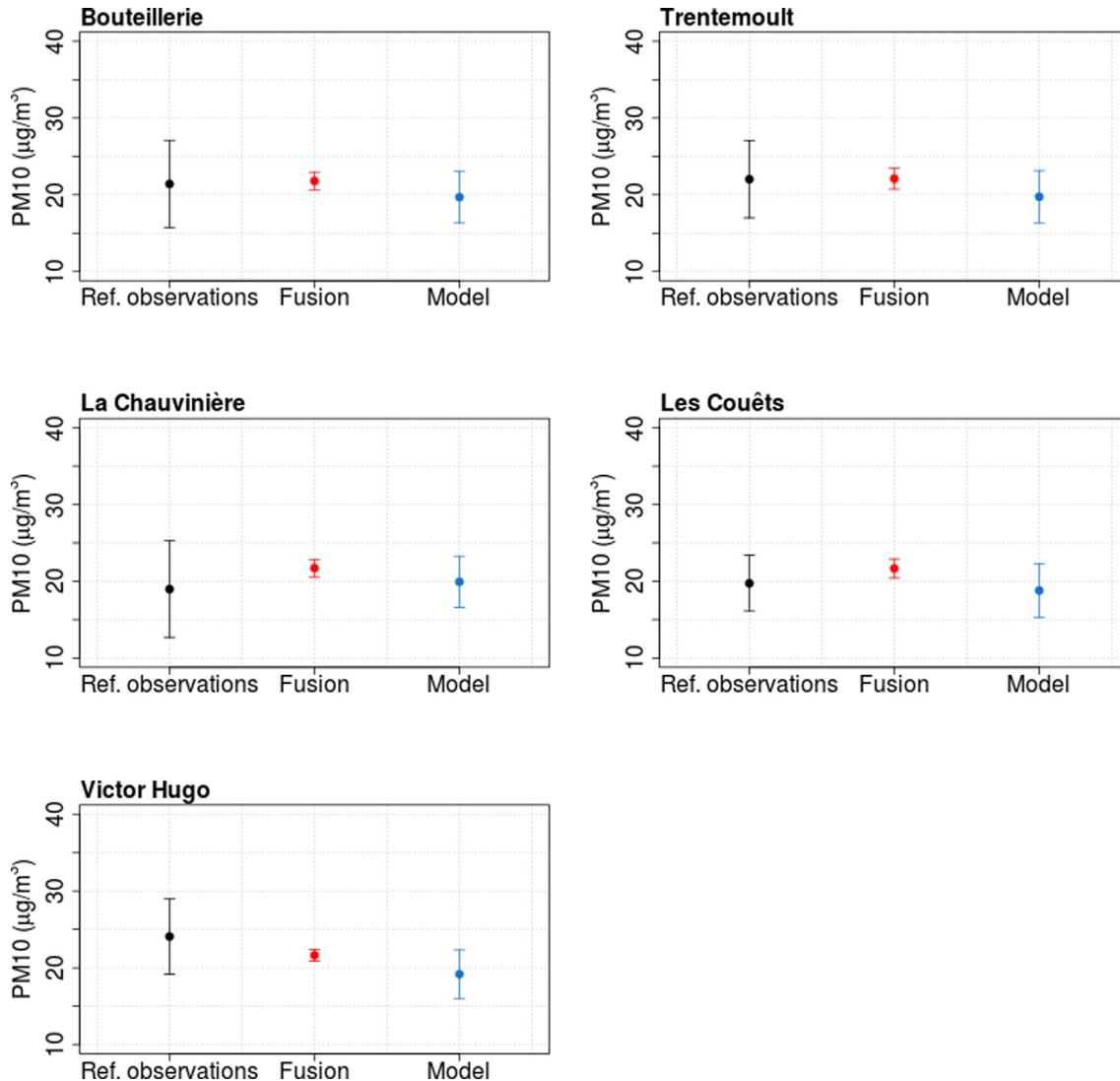


Fig. 11. The daily mean comparison between the PM₁₀ observations (in black), the data fusion (in red) and the model (ADMS-Urban, in blue) in µg/m³ at each reference station of the Air Pays de la Loire monitoring network on 11/29/2018 in Nantes.

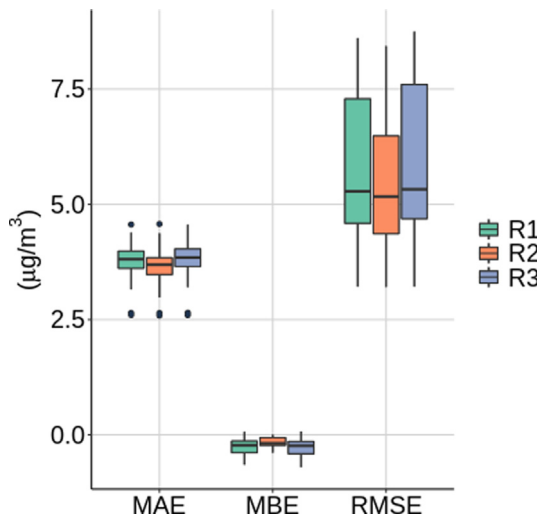


Fig. 12. The Mean Absolute Error (MAE), the Mean Bias Error (MBE) and the Root Mean Squared Error (RMSE) of the estimated PM₁₀ concentrations in Nantes on 11/29/2018 from 7 am to 7 pm derived from R1 (measurement uncertainty of 75% and 50% for mobile and fixed data, respectively), R2 (measurement uncertainty of 25% for all data) and R3 (measurement uncertainty of 150% and 100% for mobile and fixed data, respectively).

reference.

5.2.2. Impact of the sensor measurement uncertainty on the estimation

The main constraint to use sensor data in air quality mapping remains their measurement uncertainty. It has a significant effect on the data fusion approach by determining the weight allocated to the data. Sensitivity tests were carried out to quantify the effect of the measurement uncertainty on the estimation. In the previous results, a relative uncertainty was defined (75% and 50% for mobile and fixed LCS data, respectively, hereafter R1) based on the European directive and the exploratory analysis of the dataset. The sensitivity study was performed for a reduction of the initial uncertainty to the reference station uncertainty (i.e. 25%, hereafter R2) and for the doubling of the initial uncertainty (i.e. 150% and 100% for fixed and mobile sensors, respectively and hereafter R3). The performance is derived using a cross validation. It consists of leaving out one data point (i.e. the hourly average of the LCS observations at a location) at a time and determining how well this point can be estimated by external drift kriging using the other data. For the three tests (R1, R2 and R3), results are presented in Fig. 12 through boxplots of the main metrics of performance, namely the Mean Bias of Error (MBE), the Mean Absolute Error (MAE) and the Root Mean Squared Error (RMSE). These are defined as follows:

$$MBE = \frac{1}{N} \sum_{i=1}^N (z_{fusion} - z_{obs,i}) \quad (9)$$

$$MAE = \frac{1}{N} \sum_{i=1}^N |z_{fusion} - z_{obs,i}| \quad (10)$$

$$RMSE = \sqrt{\frac{1}{N} \sum_{i=1}^N (z_{fusion} - z_{obs,i})^2} \quad (11)$$

Where N is the number of observations, z_{fusion} is the estimated PM₁₀ concentration value, and $z_{obs,i}$ is the ith observed PM₁₀ concentration value. The MBE, MAE and RMSE are related by the following inequalities:

$$MBE \leq MAE \leq RMSE \leq \sqrt{N} MAE \quad (12)$$

The sensitivity study shows that by considering a measurement uncertainty for fixed and mobile LCS which is equivalent to the

reference stations (25%), the estimation of PM₁₀ concentrations by data fusion shows a slightly better performance than doubling the uncertainty (150% and 100%) or even by defining 75% and 50% for fixed and mobile sensor respectively. This suggests that to have a significant impact on air quality mapping, the accuracy of the sensors should be as good as possible.

As an illustration of the spatial difference between the data fusion from R1, R2 and R3, the related fused maps at 8 am on 11/29/2018 are given in the supplementary materials (S9). There is a maximum difference of 20 µg/m³ between R2 and R3. This highlights the importance to estimate accurately the measurement uncertainty of the devices to ensure relevant air quality mapping.

6. Conclusion

The recent technological developments in miniaturizing the instruments to measure outdoor ambient air pollution offer new possibilities for air quality monitoring and mapping. Since the reference station network is sparse and expensive, the new portable and low-cost devices could provide observations of pollutants with a higher spatial and temporal resolution. In this work, we investigated the potential added value of these data with respect to the dispersion model (ADMS-Urban) calculations for air quality mapping by applying a data fusion technique. This methodology consists in combining sensor data and dispersion model calculation to provide an estimation of pollutant concentration fields at the urban scale. The estimation of PM₁₀ concentration levels is performed in Nantes (France) on 11/29/2018 at hourly time resolution. The sensor data are provided by AtmoTrack which installs fixed and mobile sensors using driving school cars, ambulances and service vehicles as mobile platforms.

The exploratory analysis of the sensor observations demonstrates a unique sampling coverage of the city although the sampling times were limited by the drive hours. The distribution of the PM₁₀ sensor measurements are characterized by two modes that are absent on the reference observations. Those could be explained by measurements issues which are not the scope of this study. The comparison between the reference station observations and the average of 3 low-cost sensor (LCS) replicates by way of time series for the entire sampling period demonstrates good consistency even though they seem to slightly overestimate the PM₁₀ concentrations. The raw sensor dataset has been preprocessed following 2 steps. First, the unreliable data were removed from the dataset (6.5% of the mobile sensor data and 14% of the fixed sensor data were eliminated) by applying a thresholding method based on the repeatability criterion. Then, the bias related to the daily variations of the background was corrected based on the daily average of the reference station observations (AirPDL network). The corrected data were then used in the spatial interpolation to estimate the PM₁₀ concentrations in Nantes. A data fusion technique was applied combining the fixed and mobile sensor data and the 2016 annual average of the PM₁₀ concentrations calculated by the ADMS-Urban dispersion model (provided by AirPDL). Especially, an external drift kriging approach is used, and the 2016 annual average from the model is defined as the drift. In kriging, the variance of the measurement error (VME) has been considered to deal with the measurement uncertainty and the variability of the observations in the spatial interpolation. In this study, a relative measurement uncertainty is defined such as 75% and 50% of error is used for mobile and fixed sensors, respectively. The data fusion was performed hourly from 7 am to 7 pm on 11/29/2018 using the fixed and mobile sensor data. Results show that fused maps are closely related to the relative variability associated with the data points. In fact, the higher the variability is, the less the weight of the data point will be on the estimation. Thus, the estimated PM₁₀ concentrations are following the drift patterns. The estimation is also lead by the correlation between the sensor data and the drift. The better the correlation is, the lower the error related to the linear regression with the drift. In addition, kriging relies on the variogram of the residuals which gives

the variance of the residuals in space over the domain. Consequently, the response to data fusion is disparate over the day depending on this information. When the VME is low and the correlation with the drift is satisfactory, the LCS data are bringing new information to the drift patterns. Conversely, when the VME is high and/or when the correlation with the drift is not satisfactory the LCS data no longer affect the mapping. The performance of the data fusion has been investigated by comparing the daily average of the fusion, the reference observations and the model outputs at each station of the AirPDL network. The estimation by external drift kriging reduces the bias from 8% to 2% when considering LCS observations instead of the model alone. However, the estimated PM₁₀ distributions are characterized by a lower dispersion. In conclusion, the data fusion smooths the PM₁₀ concentration peaks but presents better estimate of the pollutant levels in average. In addition, the effect of the measurement uncertainty has been investigated by doubling it or reducing it to the reference station measurement uncertainty. The sensitivity tests show that the performance is increasing by reducing the uncertainty to 25% and that there is a spatial impact on the PM₁₀ concentrations fields. First, this highlights the importance to estimate accurately the measurement uncertainty of the LCS, second it demonstrates that we should be more confident in the LCS data despite their imperfections to ensure added value in air quality mapping. Among the exciting perspectives for the future, spatiotemporal kriging could be investigated to use the information in space and in time provided by the sensor data. Also, the large number of data points represents a real challenge and introduces the big data science for air quality mapping. With more than 2000 data points for an estimation period (1 h in this study), kriging calculation becomes very consuming in time and could take a lot of calculation resources. To answer this difficulty, geostatistical approaches specifically developed for large datasets such as Rivoirard and Romary, 2011, could be explored. Also, machine learning techniques, as applied in Hu and Rahman, 2017, could be investigated. These approaches allow to learn about historical observations and environmental variables and reduce significantly the computing time of the calculations. Eventually, the resulting air quality maps will be a unique support for various applications such as the estimation of the individual exposure, the communication to the citizens, the air quality monitoring, and the improvement of the pollutant emission inventories and pollution modeling.

CRediT authorship contribution statement

Alicia Gressent: Conceptualization, Methodology, Software, Validation, Writing - original draft. **Laure Malherbe:** Formal analysis, Writing - review & editing. **Augustin Colette:** Supervision, Writing - review & editing. **Hugo Rollin:** Writing - review & editing. **Romain Scimia:** Investigation.

Declaration of Competing Interest

The authors declare that they have no known competing financial interests or personal relationships that could have appeared to influence the work reported in this paper.

Acknowledgments

This work was supported by the French Ministry of Ecological and Solidarity Transition in the framework of the Central Laboratory for Air Quality Monitoring activities. We thank Air Pays de La Loire for providing the PM₁₀ reference station observations and the outputs of the ADMS-Urban model simulations for the estimation period. We also thank Laurent Spinelle, INERIS, for sharing his expertise on low cost sensors and their measurement capabilities and for his contribution in the data preprocessing development. Valuable support on the issue of measurement uncertainty was provided by Cécile Raventos, INERIS.

Appendix A. Supplementary data

Supplementary data to this article can be found online at <https://doi.org/10.1016/j.envint.2020.105965>.

References

- Alvear, O., Zamora, W., Calafate, C., Cano, J.-C., Manzoni, P., 2016. An Architecture Offering Mobile Pollution Sensing with High Spatial Resolution. *Journal of Sensors* 1458147<https://doi.org/10.1155/2016/1458147>. Article ID 1458147.
- Anenberg, S.C., Achakulwisut, P., Brauer, M., et al., 2019. Particulate matter-attributable mortality and relationships with carbon dioxide in 250 urban areas worldwide. *Sci. Rep.* 9, 11552. <https://doi.org/10.1038/s41598-019-48057-9>.
- Beauchamp, M., Malherbe, L., Létinois, L., 2010. Application de méthodes géostatistiques pour la détermination de zones de représentativité en concentration et la cartographie des dépassements de seuils. *Rapport LCSQA*.
- Beauchamp, M., Malherbe, L., Létinois, L., 2014. Estimation de l'exposition des populations aux dépassements de seuils réglementaires. *Echelle urbaine, Rapport LCSQA et annexe technique associée*.
- Beauchamp, M., Malherbe L., Meleux F., Létinois L., 2016. Note de synthèse sur les développements récents en matière de cartes analysées des résultats de modélisation. *Cartographie des concentrations de PM10 et de PM2.5. Note technique LCSQA*.
- Beauchamp, M., Malherbe, L., Létinois, L., and Drevet, J., 2017. Note de synthèse méthodologique sur la caractérisation des situations de dépassement de seuil : délimitation des zones de dépassement et estimation des populations et écosystèmes exposés. *Note technique LCSQA*.
- Beauchamp, M., Fouquet Ch. (de), Malherbe L., 2017. Dealing with non-stationarity through explanatory variables in kriging-based air quality maps. *Spatial Statistics*, 22, Part 1, 18–46.
- Beauchamp, M., Malherbe L., Fouquet Ch. (de), Létinois L., 2018. A necessary distinction between spatial representativeness of an air quality monitoring station and the delimitation of exceedance areas. *Environmental Monitoring and Assessment*, <https://doi.org/10.1007/s10661-018-6788-y>.
- Burnett, R.T., et al., 2014. An integrated risk function for estimating the global burden of disease attributable to ambient fine particulate matter exposure. *Environ. Health Perspect.* 122, 397–403.
- Burnett, R., et al., 2018. Global estimates of mortality associated with long-term exposure to outdoor fine particulate matter. *PNAS* 115 (38), 9592–9597.
- Carruthers, D.J., Edmunds, H.A., McHugh, C.A., Riches, P.J., Singles, R.J., 1997. ADMS Urban – an integrated air quality modelling system for local government, *Transactions on Ecology and the Environment*, vol. 15, ISSN 1743-3541.
- Chilès, J.-P., Delfiner, P.P., 2012. *Geostatistics: Modeling Spatial Uncertainty*. John Wiley & Sons, pp. 726.
- Cohen, A., et al., 2017. Estimates and 25-year trends of the global burden of disease attributable to ambient air pollution: An analysis of data from the global burden of diseases study 2015. *Lancet* 389, 1907–1918.
- Directive 2008/50/EC of the European Parliament and the Council of 21 May 2008 on ambient air quality and cleaner air for Europe.
- Directive 2004/107/EC of the European Parliament and the Council of 15 December 2004 on ambient air quality and cleaner air for Europe.
- European Environment Agency, 2019. Air Quality in Europe – 2019 report, EEA Report 10/2019, doi:10.2800/822355.
- Ferreira, F., Tente, H., Torres, P., Cardoso, S., Palma-Oliveira, J.M., 2000. Air quality monitoring and management in Lisbon. *Environ. Monit. Assess.* 65, 443–450.
- Fishbain, B., Lerner, U., Castell, N., Cole-Hunter, T., Popola, O., Broday, D., Iñiguez, T., et al., 2017. An evaluation tool kit of air quality micro-sensing units. *Sci Total Environ* 575, 639–648. <https://doi.org/10.1016/j.scitotenv.2016.09.061>.
- Govaerts, P., 1997. *Geostatistics for Natural Resources Evaluation*. Oxford University Press, New York, pp. 483.
- Hankey, S., Marshall, J.D., 2015. Land use regression models of on-road particulate air pollution (particle number, black carbon, PM2.5, particle size) using mobile monitoring. *Environ. Sci. Technol.* 49, 9194–9202. <https://doi.org/10.1021/acs.est.5b01209>.
- Hoek, G., Beelen, R., de Hoogh, K., Vienneau, D., Gulliver, J., et al., 2008. A review of land-use regression models to assess spatial variation of outdoor air pollution. *Atmos. Environ.* 42, 7561–7578. <https://doi.org/10.1016/j.atmosenv.2008.05.057>.
- Hu, K., Rahman, A., 2017. HazeEst: Machine Learning Based Metropolitan Air Pollution Estimation From Fixed and Mobile Sensors. *IEEE Sens. J.* 17, 3517–3525.
- Jerrett, M., Burnett, R.T., Kanaroglou, P., Eyles, J., Finkelstein, N., Giovis, C., Brook, J.R., 2001. A GIS-environmental justice analysis of particulate air pollution in Hamilton, Canada. *Environ. Plan. A* 33, 955–973.
- Jerrett, M., Arain, A., Kanaroglou, P., Beckerman, Potoglou, D., et al., 2005. A review and evaluation of intraurban air pollution exposure models. *J. Expo. Anal. Environ. Epidemiol.* 15, 185–204. <https://doi.org/10.1038/sj.jea.7500388>.
- Kumar, P., Morawska, L., Martani, C., Biskos, G., Neophytou, M., et al., 2015. The rise of low-cost sensing for managing air pollution cities. *Environ. Int.* 75, 199–205.
- Künzli, N., Jerrett, M., Mack, W.J., Beckerman, B., LaBree, L., Gilliland, F., Thomas, D., Peters, J., Hodis, H.N., 2005. Ambient air pollution and atherosclerosis in Los Angeles. *Environ. Health Perspect.* 113, 201.
- Landrigan, P.J., Fuller, R., Acost, N.J.R., Adeyi, O., Arnold, R., et al., 2017. The lancet commission on pollution and health, the Lancet.
- Lichtenstern, A., 2013. Kriging methods in spatial statistics, Bachelor's Thesis, Technische Universität München, Department of Mathematics.
- Liu, L.J.S., Rossini, A., 1996. Use of kriging models to predict 12-hour mean ozone

- concentrations in metropolitan Toronto—a pilot study. *Environ. Int.* 22, 677–692.
- Maag, B., Zhou, Z., Thiele, L., 2015. A survey on sensor calibration in air pollution monitoring deployments. *IEEE Internet Things J.* 5 (6).
- Macé, T., Mathé, F., Raventos, C., 2010. Rapport LCSQA: Recommandations techniques pour la mise en œuvre de la partie 2 du guide d'estimation des incertitudes portant sur les mesurages automatiques de SO₂, NO, NO₂, NOx, O₃ et CO réalisés sur site.
- Malherbe, L., Cárdenas, G., 2005. Application des méthodes géostatistiques pour l'exploitation conjointe des mesures de fond et de proximité. Rapport LCSQA.
- Malherbe, L., Ung, A., 2009. Travaux relatifs à la plate-forme nationale de modélisation PREV'AIR : réalisation de cartes analysées d'ozone. Rapport LCSQA.
- Malherbe, L., Wroblewski, A., Létinois, L., Rouil, L., 2010. Evaluation of numerical models used to simulate atmospheric pollution near roadways. hal-ineris.archives-ouvertes.fr.
- Minet, L., Liu, R., Valois, M.-F., Gehr, R., Xu, J., Wachenthal, S., 2018. Development and comparison of air pollution exposure surfaces derived from on-road mobile monitoring and short-term stationary sidewalk measurements. *Environ. Sci. Technol.* 2018, 52, 3512–3519. Capturing the sensitivity of land-use regression models to short-term mobile monitoring campaigns using air pollution micro-sensors. *Environ. Pollut.* 2017, 230, 280–290.
- Muller, M.D., et al., 2016. Statistical modelling of particle number concentration in Zurich at high spatio-temporal resolution utilizing data from a mobile sensor network. *Atmos. Environ.* 126, 171–181. <https://doi.org/10.1016/j.atmosenv.2015.11.033>.
- Rivoirard, J., Romary, T., 2011. Continuity for kriging with moving neighborhood. *Math. Geosci.* 43, 469–481. <https://doi.org/10.1007/s11004-011-9330-0>.
- Rouil, L., Honore, C., Vautard, R., Beekmann, M., Bessagnet, B., et al., 2009. PREV'AIR: an operational forecasting and mapping system for air quality in Europe. *Bull. Am. Meteorol. Soc.* 90 (1), 73–83.
- Ryan, P.H., LeMasters, G.K., 2007. A review of land use regression model for characterizing intraurban air pollution exposure. *Inhal Toxicol.* 19 (Suppl. 1), 127–133.
- Sack, C., Goss, C.H., 2015. It starts at the beginning: effect of particulate matter in utero. *Am. J. Respir. Crit. Care Med.* 192 (9), 1025–1026.
- Schneider, P., Castell, N., Vogt, M., Dauge, F.R., Lahoz, W.A., 2017. Mapping urban air quality in near real-time using observations from low cost sensors and model information. *Environ. Int.* 106, 234–247. <https://doi.org/10.1016/j.envint.2017.05.005>.
- Spinelle, L., Aleixandre, M., Gerboles, M., 2013. Protocol of evaluation and calibration of low-cost gas sensors for the monitoring of air pollution. European Commission, JRC Technical Reports, Report, EUR 26112 EN, 10.2788/9916.
- Spinelle, L., Gerboles, M., Villani, M.G., Aleixandre, M., Bonavatcola, F., 2015. Field calibration of a cluster of low-cost available sensors for air quality monitoring. Part A: Ozone and nitrogen dioxide. *Sens. Actuators B Chem.* 215, 249–257. <https://doi.org/10.1016/j.snb.2015.03.031>.
- Spinelle, L., Gerboles, M., Villani, M.G., Aleixandre, M., Bonavatcola, F., 2017. Field calibration of a cluster of low-cost available sensors for air quality monitoring. Part B: NO, CO and CO₂. *Sens. Actuators B Chem.* 238, 706–715. <https://doi.org/10.1016/j.snb.2016.07.036>.
- Tognet, F., 2015. Etude d'intercomparaison des modèles de qualité de l'air à l'échelle de la rue et à l'échelle urbaine. Note technique LCSA, <https://www.lcsqa.org/fr/rapport/2015/ineris/etude-intercomparaison-modeles-qualite-air-echelle-rue-echelle-urbaine>.
- Tognet, F., 2016. Etude comparative des modèles ADMS Urban et SIRANE sur un cas test. Laboratoire central de surveillance de la qualité de l'air. Retrieved December 5, 2018, from https://www.lcsqa.org/system/files/lcsqa2015-intercomparaison_adms_sirane_drc-16-667_152376-12019a_0.pdf.
- Wackernagel, H., 2003. *Multivariate Geostatistics*. Springer, Berlin Heidelbergpp, pp. 387.
- Xie, X., Semanjski, I., Gautama, S., Tsiliogianni, E., Deligiannis, N., Rajan, R.T., Pasveer, F., Philips, W.A., 2017. Review of Urban Air Pollution Monitoring and Exposure Assessment Methods. *ISPRS Int. J. Geo-Inf.* 6, 389.
- World Health Organization, 2014. Mortality and burden of disease from ambient air pollution: Situation and trends. Available at www.who.int/gho/phe/outdoor_air_pollution/.